

The effect of a guide field on local energy conversion during asymmetric magnetic reconnection: MMS observations

K. J. Genestreti,¹ J. L. Burch,² P. A. Cassak,³ R. B. Torbert,^{4,2} R. E. Ergun,^{5,6} T. D. Phan,⁷ B. L. Giles,⁸ C. T. Russell,⁹ S. Wang,¹⁰ M. Akhavan-Tafti,¹¹ R. C. Allen,^{12,2} A. Varsani¹

¹Space Research Institute, Austrian Academy of Sciences, Graz, Austria.

²Space Science and Engineering Division, Southwest Research Institute, San Antonio, TX, USA.

³West Virginia University, Morgantown, WV, USA.

⁴Space Science Center, University of New Hampshire, Durham, NH, USA.

⁵Department of Astrophysical and Planetary Sciences, University of Colorado, Boulder, CO, USA.

⁶Laboratory for Atmospheric and Space
Physics, University of Colorado, Boulder,
CO, USA.

⁷Space Science Institute, University of
California Berkeley, Berkeley, CA, USA.

⁸Heliophysics Science Division, NASA
Goddard Space Flight Center, Greenbelt,
MD, USA.

⁹University of California, Los Angeles,
CA, USA

¹⁰University of Maryland, College Park,
MD, USA

¹¹Climate and Space Sciences and
Engineering Department, University of
Michigan, Ann Arbor, MI, USA.

¹²Department of Physics and Astronomy,
University of Texas San Antonio, San
Antonio, TX, USA.

Key Points.

- For two events with $B_M \sim B_{L,sh}$, $\vec{J} \cdot \vec{E}' > 0$ at X and electron-crescent points
- For two events with $B_M \sim 0$, $\vec{J} \cdot \vec{E}' > 0$ only at electron-crescent point
- Guide fields allow electron streaming at the X-point, which takes work by the electric field

Abstract. We compare case studies of Magnetospheric Multiscale (MMS)-

observed magnetopause electron diffusion regions (EDRs) to determine how

the rate of work done by the electric field, $\vec{J} \cdot (\vec{E} + \vec{v}_e \times \vec{B}) \equiv \vec{J} \cdot \vec{E}'$,

and electron dynamics vary with magnetic shear angle. We provide an in-

depth analysis of an MMS-observed EDR event with a guide field approx-

imately the same size as the magnetosheath reconnecting field, which occurred

on 8 December 2015. We find that $\vec{J} \cdot \vec{E}'$ was large and positive near the

magnetic field reversal point, though patchy lower-amplitude $\vec{J} \cdot \vec{E}'$ also

occurred on the magnetosphere-side EDR near the electron crescent point.

The current associated with the large $\vec{J} \cdot \vec{E}'$ near the null was carried by

electrons with a velocity distribution function (VDF) resembling that of the

magnetosheath inflow, but accelerated in the anti-parallel direction by the

parallel electric field. At the magnetosphere-side EDR, the current was car-

ried by electrons with a crescent-like VDF. We compare this 8 December event

to four others with differing magnetic shear angles. This type of dual-region

$\vec{J} \cdot \vec{E}'$ was observed in another intermediate-shear EDR event, whereas the

high-shear events had a strong positive $\vec{J} \cdot \vec{E}'$ near the electron crescent

point and the low-shear event had a strong positive $\vec{J} \cdot \vec{E}'$ near the in-plane

null. We propose a physical relationship between the shear angle and mode of energy conversion where (a) a guide field provides an efficient mechanism for carrying a current at the field reversal point (streaming) and (b) a guide field may limit the formation of crescent eVDFs, limiting the current carried near the stagnation point.

1. Introduction

Magnetic reconnection is a fundamental process in plasmas. It is a change in the topology of a magnetized plasma boundary coupled with the exchange of energy from magnetic fields to particles. The topological change occurs in the electron diffusion region (EDR), wherein the electrons are demagnetized, i.e., $\vec{E} + \vec{v}_e \times \vec{B} \neq 0$. The rate of work done by the electric field on the plasma, a quantity that is often expressed in the electron rest frame as $\vec{J} \cdot (\vec{E} + \vec{v}_e \times \vec{B}) \equiv \vec{J} \cdot \vec{E}'$ [Zenitani et al., 2011], occurs in a region sometimes called the ‘dissipation region’ in order to distinguish it from the EDR [Pritchett and Mozer, 2009]. This quantity $\vec{J} \cdot \vec{E}'$ specifically represents the rate of work done on the plasma by non-ideal electric fields. Because the $\vec{E} + \vec{v}_e \times \vec{B} \neq 0$ is a defining condition for both the EDR and the $\vec{J} \cdot \vec{E}'$ region, the two regions may partially overlap; however, observations [Burch et al., 2016] and simulations [Zenitani et al., 2011] show that significant $\vec{J} \cdot \vec{E}'$ may occur several electron inertial lengths away from the magnetic X-point, where topological change occurs. Many aspects of electron-scale reconnection are not currently well understood, particularly the cause of $\vec{J} \cdot \vec{E}'$ and how, if at all, $\vec{J} \cdot \vec{E}'$ is affected by the configuration of the magnetic boundary.

Reconnection at the low-latitude magnetopause of Earth is typically asymmetric, as the plasma density in the magnetosheath, the shocked solar wind external to the magnetopause, can exceed the magnetospheric plasma density by an order of magnitude [Phan and Paschmann, 1996]. This density asymmetry alters the momentum balance equation in the vicinity of the EDR and causes the electron flow stagnation point, where there is no bulk electron motion, to be displaced from the X-point, where the magnetic field

in the reconnection plane is a minimum [Cassak and Shay, 2007]. Guide field or component reconnection occurs when the local shear angle between the magnetosheath and magnetospheric magnetic fields is less than 180° . The presence of a guide field causes the magnetic field strength at the X-point to be non-zero. The density asymmetry can lead to a displacement between the X-point and the $\vec{J} \cdot \vec{E}'$ region [Cassak and Shay, 2009; Pritchett and Mozer, 2009].

Observations of asymmetric and nearly anti-parallel reconnection have showed that field-to-plasma energy conversion and parallel electron heating occur Earthward of the X-point [Burch et al., 2016; Hwang et al., 2017]. In the central (asymmetric and anti-parallel) EDR, the current associated with $\vec{J} \cdot \vec{E}'$ is carried by electrons with perpendicular crescent-shaped velocity distribution functions (VDFs) that wrap around into the parallel direction near the stagnation point [Burch et al., 2016; Hesse et al., 2014; Shay et al., 2016]. In the outer EDR, where the Hall magnetic field is observed but electron kinetic motion still allows for non-zero \vec{E}' , parallel crescents carry the current associated with $\vec{J} \cdot \vec{E}'$ [Shay et al., 2016; Hwang et al., 2017]. The electrons may be demagnetized [Pritchett and Mozer, 2009; Hesse et al., 2014; Burch et al., 2016; Hwang et al., 2017] at the X-point, but the out-of-plane current there, a result of electron cusp motion [Shay et al., 2016], is generally weak.

Very little work has been done to determine how and why the $\vec{J} \cdot \vec{E}'$ region may change with the magnetic shear angle. [Pritchett and Mozer, 2009] compared particle-in-cell simulations of reconnection with $B_M = 0$ and $B_M = B_{L,sh}$ and found $J_{\parallel} E_{\parallel}$ at the X-point to be larger for the guide field case, though a physical explanation for this difference was not discussed. Hesse et al. [2016] showed that electron crescent VDFs also appeared near

the electron stagnation point in a simulation of guide field ($B_M \sim B_{L,sh}$) reconnection. The intensity of the crescent relative to the core of the VDF was significantly reduced in intensity as compared to their similar simulation of anti-parallel reconnection [Hesse *et al.*, 2014]. According to Hesse *et al.* [2016], crescent VDFs should reduce in intensity and eventually disappear as the guide field intensity increases to the point where the magnetic scale length $B_L/(\partial B_L \partial N)$ exceeds the electron Larmor radius, preventing mixing of electrons by thermal motion between regions with significantly different magnetic field directions.

In this study, we present a case analysis of the 8 December 2015 EDR event of Burch and Phan [2016]. We determine the electron-frame energy conversion rate and analyze the eVDFs associated with the current. We find that two of the four MMS spacecraft observed strong $\vec{J} \cdot \vec{E}' > 0$ near the in-plane magnetic null associated with E_{\parallel} -accelerated magnetosheath-inflow electrons. The eVDF is structured, with a higher-energy beam-like portion anti-aligned with the parallel electric field and a low-energy crescent-like portion aligned with E_{\parallel} . All of the four spacecraft also observed smaller positive $\vec{J} \cdot \vec{E}'$ Earthward of the in-plane null and strong negative $\vec{J} \cdot \vec{E}'$ where the high-energy beam-like portion of the eVDF wraps from the parallel direction into the $\vec{E} \times \vec{B}$ direction. The location of the $\vec{J} \cdot \vec{E}'$ region for this event is then compared to four other EDR events, which have been presented in previous studies; two with $B_M \sim 0$, one with $B_M \sim 0.5B_{L,sh}$, and one with $B_M \sim 8B_{L,sh}$. We find an apparent trend based on this limited collection of cases, where increasing the strength of the guide field appears to (a) shift the $\vec{J} \cdot \vec{E}'$ region from the electron crescent point toward the in-plane null point and (b) reduce the intensity of the electron crescent VDFs.

In the following section we describe the MMS instrumentation and data analysis techniques used in this study. In section 3 we present our case analysis of the 8 December 2015 EDR event. In section 4 we compare the 8 December 2015 event to the two high-shear ($B_M \sim 0$) events of *Burch et al.* [2016] and *Hwang et al.* [2017]. In section 5 we compare the 8 December 2015 event to another intermediate-shear ($B_M/B_{L,sh} \sim 0.5$) event and to the large guide field event of *Eriksson et al.* [2016]. In the final section we summarize our results and discuss the possible implications of our case comparisons and open questions.

2. Instrumentation and data

This study analyzes burst-mode data from the suite of plasma particle and field instruments onboard MMS [*Burch et al.*, 2016]. The fast plasma investigation (FPI) dual ion and electron spectrometers (DIS and DES, respectively) measure differential directional fluxes for their namesake particle species at 32 energies between ~ 10 eV/ q and ~ 28 keV/ q [*Pollock et al.*, 2016]. FPI-DIS and DES provide 4π -steradian velocity distribution functions (VDFs) once every 150 ms and 30 ms, respectively. The DC magnetic field vector is measured by the fluxgate magnetometers (FGM) at 128 samples per second [*Russell et al.*, 2016]. The AC magnetic field vector is measured by the search coil magnetometers (SCM) at a rate of 8196 samples per second [*Le Contel et al.*, 2016], as are the spin-plane [*Lindqvist et al.*, 2016] and axial [*Ergun et al.*, 2016] components of the electric field, which are measured by two sets of probes collectively referred to as the electric field double probes (EDP). All of the data used in this study are available through the MMS science data center (<https://lasp.colorado.edu/mms/sdc/public/>).

Some of the data are resampled and/or smoothed prior to analysis. For instance, we have shifted all FPI data forward by half of an acquisition period (75 ms for DIS and 15

ms for DES), such that the time stamps mark the average time, rather than the beginning, of an acquisition period. We have also smoothed the AC electric field data using a sliding overlapping boxcar scheme, where the width of the boxcar (± 30 ms) was chosen to match the sample rate of FPI-DES and provide the best possible agreement between \vec{E} and $-\vec{v}_e \times \vec{B}$. Smoothing the electric field reduces the magnitude of positive and negative oscillations of $\vec{J} \cdot \vec{E}'$, but makes the bulk action of the electric field on the plasma more easily discernible. For cases where 4-spacecraft data are analyzed simultaneously, e.g., for the curlometer technique, we have used linear interpolation in time to obtain data from MMS2, 3, and 4 with the same time stamps as the corresponding dataset from MMS1. We also perform linear interpolations in space to estimate gradients, divergences, curls, and multi-spacecraft averages, as in *Chanteur* [1998].

All data is shown in either magnetopause-normal (LMN) or field-aligned (FAC) coordinates. The LMN eigenvector system for the 8 December 2015 event is taken from *Burch and Phan* [2016], which was determined using minimum variance and minimization of Faraday residue [*Khrabrov and Sonnerup*, 1998]. The coordinate axes, \hat{L} , \hat{M} , and \hat{N} are constant in time and defined in a GSE basis as $[0.3641, -0.1870, 0.9124]$, $[-0.2780, -0.9568, 0.08515]$, and $[0.8889, -0.2226, -0.4003]$, respectively. \hat{L} is the direction of maximum magnetic variance and the reconnection outflow. \hat{M} is the direction of intermediate variance and the guide and Hall magnetic fields. \hat{N} is the direction of minimum variance, the magnetopause normal, and the reconnection inflow. For FAC, the coordinate axes are calculated for each magnetic field measurement and are defined as \hat{v}_{\parallel} , $\hat{v}_{\perp 1}$, and $\hat{v}_{\perp 2}$, which are defined as \hat{b} , $(\hat{b} \times \hat{v}_e) \times \hat{b}$, and $\hat{b} \times \hat{v}_e$, respectively, where \hat{b} is the direction of the magnetic field and \hat{v}_e is the direction of the electron bulk velocity.

3. Analysis of the 8 December 2015 EDR event

An overview of MMS data for the 8 December 2015 event is provided in *Burch and Phan* [2016]. We focus on the single ~ 2 -second magnetopause crossing from approximately 11:20:43 – 11:20:45 UT. For the hour prior to this interval, the interplanetary magnetic field propagated to the bow shock was weakly south, with a mean value of $B_Z = -1 \text{ nT} \pm 1 \text{ nT}$ and a mean clock angle of $120^\circ \pm 30^\circ$. Geomagnetic activity for the day was minimal, with a maximum Kp of 3 and a near-zero Dst. The local shear angle at the magnetopause, which was observed near the subsolar point, was approximately 115° , with southward and dawnward components of the magnetosheath magnetic field of $B_L \approx B_M \approx -20 \text{ nT}$. The magnetopause crossed the spacecraft at roughly 44 km/s in the normal direction [Burch and Phan, 2016]. The spacecraft exited the magnetosheath, crossed the boundary layer, and entered the magnetosphere, led by MMS3, then followed by MMS2 and MMS1 nearly simultaneously, and lastly by MMS4. The formation of the four spacecraft for this magnetopause crossing is shown in Figure 1.

Figure 2 shows data from MMS2 for this event. Similar data for MMS1–4 are also found in Movies 1–4. Seven relevant times are marked on Figure 2 by the vertical lines labeled $t_1 - t_7$. Two regions of large duskward currents ($J_M < 0$) are seen between t_1 and t_2 , near the in-plane-null, and between $t_3 - t_4$, on the magnetosphere side of the EDR [Burch and Phan, 2016]. Between t_1 and t_3 the in-plane current is directed southward ($J_L < 0$) carried by electrons flowing away from the central EDR and between t_3 and t_6 the in-plane current is largely directed northward. These in-plane currents are in the expected direction of the Hall currents [Pritchett, 2008], which are consistent with the large negative deflection of B_M near t_2 and the relatively smaller positive deflection of

B_M between t_4 and t_6 . The first and last currents associated with the deflected B_M field (Hall field) are seen at t_1 and t_5 , and are likely close to the field lines that were actively reconnecting (the separatrices). The time difference between points t_1 and t_6 is approximately 1.1 seconds, which, for an assumed-constant boundary velocity of 44 km/s in the normal direction, implies that the thickness of the reconnection layer from the magnetosheath-side separatrix to the magnetosphere-side separatrix is ~ 48 km, or roughly 26 electron inertial lengths ($d_{e,sh} \approx 1.88$ km) and less than half of one ion inertial length ($d_{i,sh} \approx 102$ km).

As indicated by Figure 2f–h, the ions become demagnetized near t_1 and remain demagnetized well past the magnetospheric edge of the EDR. The smoothed (\sim DC) electric field, shown in blue, is almost completely balanced by the electron convective electric field, shown in red, except for a brief interval near the in-plane null and first large out-of-plane current ($\sim t_1$) and throughout the second region of large out-of-plane current ($\sim t_3 - t_6$). The large discrepancy between E_N and $(-\vec{v}_e \times \vec{B})_N$ is likely caused by a drift of the baseline of the EDP, as the plasma conditions change rapidly and dramatically throughout this interval [Eriksson *et al.*, 2016]. The DC electric field vector is also significantly smaller than the peak-to-peak AC electric field, which has large-amplitude oscillations near the in-plane null ($\sim t_2$) and on the magnetosphere side of the boundary layer roughly between t_3 and t_7 .

$\vec{J} \cdot \vec{E}'$ is shown in black in Figure 2i. Because the large value of E'_N may be an instrumental effect, the sum $J_L E'_L + J_M E'_M$ is also shown in grey in the same panel. The dominant non-zero features appear at t_2 and t_4 , where $\vec{J} \cdot \vec{E}'$ was approximately $+10$ nW/m³ and -5 nW/m³, respectively, and is visibly unaffected by the baseline drift in E_N . The cuts

of the eVDFs to the right of the stack plot in Figure 2 show the portions of the eVDFs that carry the currents at t_2 (Figure 2k–n) and t_4 (Figure 2o–r). (Note that the full set of eVDFs for each of the 4 spacecraft can be found in Movies 1–4.)

At t_2 , which is where the largest current was observed near the in-plane null, the eVDF appears to be reasonably well organized by magnetic field coordinates. There is a beam-like portion of the eVDF streaming nearly anti-parallel to the guide field, balanced partially by a lower-energy crescent-like portion of inflowing electrons. The beam-like portion of the eVDF is anti-aligned with \vec{E}'_{\parallel} and is likely formed by acceleration from the out-of-plane reconnection electric field. The net current is aligned with \vec{E}' , as indicated by the net-positive $\vec{J} \cdot \vec{E}'$ of ~ 10 nW/m³.

Between t_2 and t_3 , dubbed a “quiescent region” by *Burch and Phan* [2016], the beam-like anti-parallel portion of the eVDF persists, but at reduced energies where it is balanced by the parallel portion of the eVDF. The apparent isotropization of electrons in the quiescent region (Figure 2j) may be a result of pitch-angle scattering of inflowing sheath electrons by highly curved field lines near the null [*Lavraud et al.*, 2016]. Near t_3 , the parallel portion of the eVDF is reduced in intensity (see Movie 2). At t_4 , the eVDF is not well organized by magnetic field coordinates (though the eVDFs measured immediately before and after t_4 do appear to be organized by \vec{B}). Here the enhanced anti-parallel portion of the eVDF turns from the \hat{v}_{\parallel} to the $\hat{v}_{\perp 1}$ direction (Figures 2l and 2p) and becomes partially aligned with \vec{E}' , resulting in a net generation of electromagnetic energy with $\vec{J} \cdot \vec{E}' \approx -6$ nW/m³. *Hwang et al.* [2017] reported negative values of $\vec{J} \cdot \vec{E}'$ during an MMS-observed EDR (this event will be discussed in the next section) and concluded that it was associated with the breaking of a super-Alfvenic electron jet in the outer EDR. It is possible that this may

also explain the large negative $\vec{J} \cdot \vec{E}'$ for this 8 December event, as the large negative B_M and the strong positive-to-negative reversal in $V_{e,L}$ seen in this event are consistent with an anti-normal-directed crossing of the southward EDR [Shay *et al.*, 2016]. However, it is worth noting that the negative peak in $\vec{J} \cdot \vec{E}'$ for this event is much more narrow than the negative $\vec{J} \cdot \vec{E}'$ observed by Hwang *et al.* [2017].

Figure 3 shows $\vec{J} \cdot \vec{E}'$ for each of the four spacecraft, as well as the magnetic field vectors. A comparison between Figures 3b, 3d, 3f, and 3h reveals that the $\vec{J} \cdot \vec{E}'$ region for this event is highly structured within the approximately $25 d_{e,sh}$ -thick region between the magnetosheath-side and magnetosphere-side separatrices. Each of the spacecraft observed $\vec{J} \cdot \vec{E}' > 0$ of some magnitude immediately Earthward of the field reversal point, though the electron-frame energy conversion rates observed by MMS1 and MMS3 were approximately half as large as those observed by MMS2 and MMS4. The structure of $\vec{J} \cdot \vec{E}'$ on the Earthward side of the EDR differed drastically for the four spacecraft, indicating patchy (in time and/or space) energy exchange between the fields and plasma. Each of the 4 spacecraft saw similar eVDFs near the field reversal point, which consisted of a higher-energy anti-parallel beam and a lower-energy parallel crescent. Each of the 4 spacecraft also observed large negative $\vec{J} \cdot \vec{E}'$ associated with the turning of the anti-parallel beam into the positive $\hat{v}_{\perp 1}$ direction. On all but MMS4, these turning eVDFs and large negative values of $\vec{J} \cdot \vec{E}'$ were observed on the Earthward side of the quiescent region during the second of the two current peaks where $n_e > n_i$. The duration and consistent measurement of this density imbalance by multiple spacecraft suggests that it is not an artifact caused by differences in the operation of FPI-DES and DIS, e.g., differences in the sample rate and/or calibration, though any physical link between this density imbalance and the $\vec{J} \cdot \vec{E}'$

is not known. Full sets of eVDF cuts for this interval for each spacecraft are shown in Movies 1–4.

4. Energy conversion in high-shear EDR events

Figure 4 shows data from MMS-1 and 3 for two very high-shear EDR events, which were identified and characterized in detail in *Burch et al.* [2016] (Figure 4 left-hand side) and *Hwang et al.* [2017] (Figure 4 right-hand side). The vertical dashed red line indicates the point where $\vec{J} \cdot \vec{E}'$ is largest and the vertical dashed blue line indicates where the spacecraft was close to the magnetic null. For both events, the magnetopause contracted inward across MMS. The direction of the effective spacecraft velocity was approximately aligned with the normal, such that MMS observed both the $B_L = B_N = 0$ point and crescent-shaped velocity distribution functions. The magnetic shear angle was approximately 170° for the 16 October event [*Burch et al.*, 2016] and 153° for the 19 September event [*Hwang et al.*, 2017].

The separation between the $\vec{J} \cdot \vec{E}'$ peaks and the $B_L = 0$ points were well-resolved for both of these events. For the 16 October event, eight eVDFs were collected between the null and the $\vec{J} \cdot \vec{E}'$ peak. Eighteen eVDFs were collected between these points for the 19 September event. For both events, the current at the $\vec{J} \cdot \vec{E}'$ peak was carried by crescent-shaped eVDFs. For the inner-EDR event of 16 October, both parallel and perpendicular crescents were observed, while only parallel crescents were observed for the outer-EDR event of 19 September. Figure 4c and 4f show that no parallel electron heating was occurring near the B_L reversal, while the parallel electron temperature was significantly larger than the perpendicular temperature near and Earthward of the $\vec{J} \cdot \vec{E}'$ peak.

5. Energy conversion in intermediate and low-shear EDR events

Figure 5 shows data from two component-reconnection EDR events. The first event, shown in 5a–c, was observed during a roughly 30-second magnetopause crossing. There was a guide field approximately half as large as the reconnecting component of the magnetosheath field. Crescent-shaped eVDFs (Figure 5g) were observed near 7:36:37–7:36:39 UT (vertical dashed red line in Figure 5a–c). The parallel crescents carried a northward current of $\sim 0.5 \mu\text{A}/\text{m}^2$, which was co-located with a parallel electric field of $\leq 10 \text{ mV}/\text{m}$. At the field reversal point (vertical dashed blue line in Figure 5a–c), there was an intense out-of-plane current of $\sim 2 \mu\text{A}/\text{m}^2$ co-located with a parallel electric field of $\leq 6 \text{ mV}/\text{m}$. The current at the field reversal point was carried by magnetosheath-inflow-like eVDFs, which were accelerated in the anti-parallel direction by the parallel electric field. After smoothing the high-resolution electric field data (similar to Figures 2 and 3), we calculated $\vec{J} \cdot \vec{E}' \leq 1 \text{ nW}/\text{m}^3$. For this event, the large time difference between the appearance of the crescent eVDFs and the field reversal point meant that the two points were separated by roughly 615 eVDF measurements. The electrons were demagnetized at both the field reversal and crescent eVDF points, where parallel electron heating was also observed. This type of dual-region reconnection is comparable to what was observed for the 8 December event, though $\vec{J} \cdot \vec{E}'$ was smaller in intensity by a factor of ~ 10 (despite the fact that the upstream conditions for these two events were similar).

The right-hand side of Figure 5 shows data from the very low-shear ($B_M/B_{L,sh} \sim 8$) EDR event of *Eriksson et al.* [2016]. For this event, the EDR was observed within a Kelvin-Helmholtz vortex created by the flow shear of the magnetosheath at the dusk flank of the magnetopause. The asymptotic plasma density in the magnetosheath was approximately

2.5 times larger than the asymptotic magnetospheric density, which is comparable in magnitude to the density asymmetry for the 8 December event. No crescent-shaped eVDFs were observed for this event, which may be a result of a reduction in the Larmor radius by the intense guide field [Hesse *et al.*, 2016]. Strong electron-frame energy conversion was observed at the in-plane magnetic null and nowhere else. At the in-plane null, the current was carried by magnetosheath-inflow-like eVDFs that were accelerated in the parallel direction by an anti-parallel ($-\hat{M}$) electric field.

6. Summary and discussion

6.1. Summary

We have analyzed, in detail, the electron-frame energy conversion rate $\vec{J} \cdot (\vec{E} + \vec{v}_e \times \vec{B}) \equiv \vec{J} \cdot \vec{E}'$ that occurred during the intermediate-shear ($B_M/B_{L,sh} \sim 1$) 8 December 2015 EDR event. We found that the $\vec{J} \cdot \vec{E}'$ region was highly structured. MMS-2 and 4 observed $\vec{J} \cdot \vec{E}' \approx 10$ nW/m³ near the in-plane magnetic null point. All four spacecraft observed smaller, patchy $|\vec{J} \cdot \vec{E}'| \leq 5$ nW/m³ Earthward of the magnetic null, and strong $\vec{J} \cdot \vec{E}' \approx -10$ nW/m³ near the Earthward edge of the EDR. The strong positive $\vec{J} \cdot \vec{E}'$ was associated with a current carried by an anti-parallel beam-like portion of the eVDF, which was partially balanced by a lower-energy anti-parallel magnetosheath-inflow-like portion of the eVDF. The strong negative $\vec{J} \cdot \vec{E}'$ was associated with the turning of this beam into the $\hat{v}_{\perp 1}$ direction.

In sections 4 and 5 we reproduced similar analyses for four additional EDR events with differing magnetic shear angles, three of which have been identified and characterized in past studies. For two anti-parallel events, we showed that the $\vec{J} \cdot \vec{E}'$ peaks were separated by

a small but well-resolved distance from the magnetic null points, as was shown previously in *Burch et al.* [2016] and *Hwang et al.* [2017].

For the EDR event of 28 November 2016, which we have classified as an intermediate-shear reconnection event, we found that strong positive $\vec{J} \cdot \vec{E}'$ and parallel electron heating were observed near the in-plane null and the crescent-eVDF points. The current at the null was carried by magnetosheath-inflow-like eVDFs accelerated in the anti-parallel ($+\hat{M}$) direction by a parallel ($-\hat{M}$) electric field.

Lastly, for the large guide field event of *Eriksson et al.* [2016], we demonstrated that strong positive $\vec{J} \cdot \vec{E}'$ and parallel electron heating occurred only at the null. Again, the out-of-plane current was carried by magnetosheath-inflow-like eVDFs, accelerated in the parallel ($+\hat{M}$) direction by an anti-parallel ($-\hat{M}$) electric field.

6.2. Interpretation: influence of shear angle on energy conversion

From this collection of cases it appears that the introduction of a guide field enhances $\vec{J} \cdot \vec{E}'$ at the in-plane magnetic null, which is similar to a result of *Pritchett and Mozer* [2009], as discussed in the first section of this paper. The possible mechanism for this switching is easily explained. The introduction of a guide field causes the magnetic field at the X-point to be non-zero, allowing for free streaming of the electrons along the guide field due to the out-of-plane reconnection electric field. This is consistent with the eVDFs near the in-plane null points from the intermediate-to-low-shear EDR events of 28 November 2016, 8 December 2015, and 8 September 2015, which had guide fields 0.5, 1, and 8 times as large as $B_{L,sh}$, respectively. For these events, the current near the in-plane null point and at the $\vec{J} \cdot \vec{E}'$ peak was carried by electrons with magnetosheath-inflow-like VDFs shifted in the $+\hat{M}$ direction by a $-\hat{M}$ reconnection electric field. There was

significant structure to the eVDF near the in-plane null for the 8 December event, which did not appear in the eVDFs for the other two aforementioned events. This structured eVDF may be a result of the larger parallel electric field for the 8 December event, which was roughly 10 and 4.3 times the size of the parallel electric field for the 28 November and 8 September events, respectively.

There is also an apparent trend, based on these few events, where increasing the guide field reduces $\vec{J} \cdot \vec{E}'$ near the electron stagnation point (where crescent-eVDFs are observed). In the 28 November event, with $B_M \sim 0.5B_L$, strong parallel crescents were observed. In the 8 December event, with $B_M \sim B_L$, weaker parallel and perpendicular crescents were observed [Burch and Phan, 2016]. No crescents were observed for the 8 September event [Eriksson et al., 2016]. Increasing the strength of the guide field may reduce the intensity of the crescents, which are a result of finite gyroradius effects [Hesse et al., 2014], by reducing the ratio of the gyroradius to the skin depth. It should be noted, however, that the density asymmetry for these events was not uniform. The density ratios n_{sh}/n_{sp} for the 8 December and 8 September events were 2.5, whereas the density ratio for the 28 November event was ~ 10 .

6.3. Future work

This study was based on a small set of events. A more comprehensive analysis and characterization of EDR events with varying guide field strengths should be conducted to confirm or refute the interpretation provided in the previous section. Additional low-shear EDRs should be identified and/or included in this analysis. As of yet, to the knowledge of the authors, there has only been one very low-shear EDR event identified in the MMS

data. This limited number of events may be explained if (a) the guide field suppresses crescent formation and (b) crescents are being used to identify EDRs.

Another pressing question is related to strength of the density asymmetry. The density asymmetries varied between these events and, as discussed previously, separation of the X-point and the stagnation points and crescent formation are both consequences of asymmetric reconnection. This question may be most easily addressed with simulations, where all of the parameters for a reconnection event may be pre-defined.

We have largely introduced the differences between $\vec{J} \cdot \vec{E}'$ for low and high-shear reconnection in a phenomenological manner, so there are many open questions related to the underlying physics that should create these differences. The mechanism for electron acceleration near the in-plane null during component reconnection and the parameters that govern the separation between $\vec{J} \cdot \vec{E}'$ peaks for intermediate-shear reconnection are both unknown. It is also unknown why, despite having similar upstream conditions, $\vec{J} \cdot \vec{E}'$ was an order of magnitude smaller for the 28 November event than for the 8 December and 9 September events.

Acknowledgments. The authors would like to thank everyone who contributed to the success of the MMS mission and those who contributed to the rich scientific heritage on which this mission is based. This work was funded by the Austrian Academy of Sciences FFG project number 847069. Kevin Genestreti would like to thank Rumi Nakamura, Yasuhito Narita, Stephen Fuselier, and Jerry Goldstein for helpful conversations. The MMS data are publicly available at <https://lasp.colorado.edu/mms/sdc/public>. Kp index data are available at

ftp://ftp.ngdc.noaa.gov/STP/GEOMAGNETIC_DATA/INDICES/KP_AP, and Dst data are available at <http://wdc.kugi.kyoto-u.ac.jp>.

References

- Burch, J. L., and T. D. Phan (2016), Magnetic reconnection at the dayside magnetopause: Advances with MMS, *Geophys. Res. Lett.*, *43*, 8327–8338, doi:10.1002/2016GL069787.
- Burch, J. L., R. B. Torbert, T. D. Phan, L.-J. Chen, T. E. Moore, R. E. Ergun, J. P. Eastwood, D. J. Gershman, P. A. Cassak, M. R. Argall, S. Wang, M. Hesse, C. J. Pollock, B. L. Giles, R. Nakamura, B. H. Mauk, S. A. Fuselier, C. T. Russell, R. J. Strangeway, J. F. Drake, M. A. Shay, Y. V. Khotyaintsev, P.-A. Lindqvist, G. Marklund, F. D. Wilder, D. T. Young, K. Torkar, J. Goldstein, J. C. Dorelli, L. A. Avanov, M. Oka, D. N. Baker, A. N. Jaynes, K. A. Goodrich, I. J. Cohen, D. L. Turner, J. F. Fennell, J. B. Blake, J. Clemmons, M. Goldman, D. Newman, S. M. Petriner, K. J. Trattner, B. Lavraud, P. H. Reiff, W. Baumjohann, W. Magnes, M. Steller, W. Lewis, Y. Saito, V. Coffey, and M. Chandler (2016), Electron-scale measurements of magnetic reconnection in space, *Science*, doi:10.1126/science.aaf2939.
- Burch, J. L., T. E. Moore, R. B. Torbert, and B. L. Giles (2016), Magnetospheric Multi-scale Overview and Science Objectives, *Spa. Sci. Rev.*, *199*, 5–21, doi:10.1007/s11214-015-0164-9.
- Cassak, P. A., and M. A. Shay (2007), Scaling of asymmetric magnetic reconnection: General theory and collisional simulations, *Physics of Plasmas*, *14*(10), 102114, doi:10.1063/1.2795630.

- Cassak, P. A., and M. A. Shay (2009), Structure of the dissipation region in fluid simulations of asymmetric magnetic reconnection, *Physics of Plasmas*, *16*(5), 055,704, doi:10.1063/1.3086867.
- Chanteur, G. (1998), Spatial Interpolation for Four Spacecraft: Theory, in *Analysis Methods for Multi-Spacecraft Data*, edited by G. Paschmann and P. W. Daly, chap. 14, pp. 349–368, International Space Science Institute.
- Ergun, R. E., S. Tucker, J. Westfall, K. A. Goodrich, D. M. Malaspina, D. Summers, J. Wallace, M. Karlsson, J. Mack, N. Brennan, B. Pyke, P. Withnell, R. Torbert, J. Macri, D. Rau, I. Dors, J. Needell, P.-A. Lindqvist, G. Olsson, and C. M. Cully (2016), The Axial Double Probe and Fields Signal Processing for the MMS Mission, *Spa. Sci. Rev.*, *199*, 167–188, doi:10.1007/s11214-014-0115-x.
- Eriksson, S., F. D. Wilder, R. E. Ergun, S. J. Schwartz, P. A. Cassak, J. L. Burch, L.-J. Chen, R. B. Torbert, T. D. Phan, B. Lavraud, K. A. Goodrich, J. C. Holmes, J. E. Stawarz, A. P. Sturner, D. M. Malaspina, M. E. Usanova, K. J. Trattner, R. J. Strangeway, C. T. Russell, C. J. Pollock, B. L. Giles, M. Hesse, P.-A. Lindqvist, J. F. Drake, M. A. Shay, R. Nakamura, and G. T. Marklund (2016), Magnetospheric Multiscale Observations of the Electron Diffusion Region of Large Guide Field Magnetic Reconnection, *Phys. Rev. Lett.*, *117*(1), 015001, doi:10.1103/PhysRevLett.117.015001.
- Hesse, M., N. Aunai, D. Sibeck, and J. Birn (2014), On the electron diffusion region in planar, asymmetric, systems, *Geophys. Res. Lett.*, *41*, 8673–8680, doi:10.1002/2014GL061586.
- Hesse, M., Y.-H. Liu, L.-J. Chen, N. Bessho, M. Kuznetsova, J. Birn, and J. L. Burch (2016), On the electron diffusion region in asymmetric reconnection with a guide mag-

netic field, *Geophys. Res. Lett.*, *43*, 2359–2364, doi:10.1002/2016GL068373.

Hwang, K.-J., D. G. Sibeck, E. Choi, L.-J. Chen, R. E. Ergun, Y. Khotyaintsev, B. L. Giles, C. J. Pollock, D. Gershman, J. C. Dorelli, L. Avanov, W. R. Paterson, J. L. Burch, C. T. Russell, R. J. Strangeway, and R. B. Torbert (2017), Magnetospheric multiscale mission observations of the outer electron diffusion region, *Geophysical Research Letters*, pp. n/a–n/a, doi:10.1002/2017GL072830, 2017GL072830.

Khrabrov, A. V., and B. U. Ö. Sonnerup (1998), Orientation and motion of current layers: minimization of the Faraday residue, *Geophys. Res. Lett.*, *25*, 2373–2376, doi:10.1029/98GL51784.

Lavraud, B., Y. C. Zhang, Y. Vernisse, D. J. Gershman, J. Dorelli, P. A. Cassak, J. Dargent, C. Pollock, B. Giles, N. Aunai, M. Argall, L. Avanov, A. Barrie, J. Burch, M. Chandler, L.-J. Chen, G. Clark, I. Cohen, V. Coffey, J. P. Eastwood, J. Egedal, S. Eriksson, R. Ergun, C. J. Farrugia, S. A. Fuselier, V. Génot, D. Graham, E. Grigorenko, H. Hasegawa, C. Jacquety, I. Kacem, Y. Khotyaintsev, E. MacDonald, W. Magnes, A. Marchaudon, B. Mauk, T. E. Moore, T. Mukai, R. Nakamura, W. Paterson, E. Penou, T. D. Phan, A. Rager, A. Retino, Z. J. Rong, C. T. Russell, Y. Saito, J.-A. Sauvaud, S. J. Schwartz, C. Shen, S. Smith, R. Strangeway, S. Toledo-Redondo, R. Torbert, D. L. Turner, S. Wang, and S. Yokota (2016), Currents and associated electron scattering and bouncing near the diffusion region at Earth’s magnetopause, *Geophys. Res. Lett.*, *43*, 3042–3050, doi:10.1002/2016GL068359.

Le Contel, O., P. Leroy, A. Roux, C. Coillot, D. Alison, A. Bouabdellah, L. Mirioni, L. Meslier, A. Galic, M. C. Vassal, R. B. Torbert, J. Needell, D. Rau, I. Dors, R. E. Ergun, J. Westfall, D. Summers, J. Wallace, W. Magnes, A. Valavanoglou, G. Olsson,

- M. Chutter, J. Macri, S. Myers, S. Turco, J. Nolin, D. Bodet, K. Rowe, M. Tanguy, and B. de la Porte (2016), The Search-Coil Magnetometer for MMS, *Spa. Sci. Rev.*, *199*, 257–282, doi:10.1007/s11214-014-0096-9.
- Lindqvist, P.-A., G. Olsson, R. B. Torbert, B. King, M. Granoff, D. Rau, G. Needell, S. Turco, I. Dors, P. Beckman, J. Macri, C. Frost, J. Salwen, A. Eriksson, L. Åhlén, Y. V. Khotyaintsev, J. Porter, K. Lappalainen, R. E. Ergun, W. Wermeer, and S. Tucker (2016), The Spin-Plane Double Probe Electric Field Instrument for MMS, *Spa. Sci. Rev.*, *199*, 137–165, doi:10.1007/s11214-014-0116-9.
- Phan, T. D., and G. Paschmann (1996), Low-latitude dayside magnetopause and boundary layer for high magnetic shear: 1. structure and motion, *Journal of Geophysical Research: Space Physics*, *101*(A4), 7801–7815, doi:10.1029/95JA03752.
- Pollock, C., T. Moore, A. Jacques, J. Burch, U. Gliese, Y. Saito, T. Omoto, L. Avanov, A. Barrie, V. Coffey, J. Dorelli, D. Gershman, B. Giles, T. Rosnack, C. Salo, S. Yokota, M. Adrian, C. Aoustin, C. Auletta, S. Aung, V. Bigio, N. Cao, M. Chandler, D. Chornay, K. Christian, G. Clark, G. Collinson, T. Corris, A. De Los Santos, R. Devlin, T. Diaz, T. Dickerson, C. Dickson, A. Diekmann, F. Diggs, C. Duncan, A. Figueroa-Vinas, C. Firman, M. Freeman, N. Galassi, K. Garcia, G. Goodhart, D. Guererro, J. Hageman, J. Hanley, E. Hemminger, M. Holland, M. Hutchins, T. James, W. Jones, S. Kreisler, J. Kujawski, V. Lavu, J. Lobell, E. LeCompte, A. Lukemire, E. MacDonald, A. Mariano, T. Mukai, K. Narayanan, Q. Nguyen, M. Onizuka, W. Paterson, S. Persyn, B. Piepgrass, F. Cheney, A. Rager, T. Raghuram, A. Ramil, L. Reichenthal, H. Rodriguez, J. Rouzaud, A. Rucker, Y. Saito, M. Samara, J.-A. Sauvaud, D. Schuster, M. Shapirio, K. Shelton, D. Sher, D. Smith, K. Smith, S. Smith, D. Steinfeld, R. Szymkiewicz,

- K. Tanimoto, J. Taylor, C. Tucker, K. Tull, A. Uhl, J. Vloet, P. Walpole, S. Weidner, D. White, G. Winkert, P.-S. Yeh, and M. Zeuch (2016), Fast Plasma Investigation for Magnetospheric Multiscale, *Spa. Sci. Rev.*, *199*, 331–406, doi:10.1007/s11214-016-0245-4.
- Pritchett, P. L. (2008), Collisionless magnetic reconnection in an asymmetric current sheet, *Journal of Geophysical Research: Space Physics*, *113*(A6), n/a–n/a, doi:10.1029/2007JA012930, a06210.
- Pritchett, P. L., and F. S. Mozer (2009), The magnetic field reconnection site and dissipation region, *Physics of Plasmas*, *16*(8), 080702, doi:10.1063/1.3206947.
- Russell, C. T., B. J. Anderson, W. Baumjohann, K. R. Bromund, D. Dearborn, D. Fischer, G. Le, H. K. Leinweber, D. Leneman, W. Magnes, J. D. Means, M. B. Moldwin, R. Nakamura, D. Pierce, F. Plaschke, K. M. Rowe, J. A. Slavin, R. J. Strangeway, R. Torbert, C. Hagen, I. Jernej, A. Valavanoglou, and I. Richter (2016), The Magnetospheric Multiscale Magnetometers, *Spa. Sci. Rev.*, *199*, 189–256, doi:10.1007/s11214-014-0057-3.
- Shay, M. A., T. D. Phan, C. C. Haggerty, M. Fujimoto, J. F. Drake, K. Malakit, P. A. Cassak, and M. Swisdak (2016), Kinetic signatures of the region surrounding the X line in asymmetric (magnetopause) reconnection, *Geophys. Res. Lett.*, *43*, 4145–4154, doi:10.1002/2016GL069034.
- Zenitani, S., M. Hesse, A. Klimas, and M. Kuznetsova (2011), New Measure of the Dissipation Region in Collisionless Magnetic Reconnection, *Physical Review Letters*, *106*(19), 195003, doi:10.1103/PhysRevLett.106.195003.

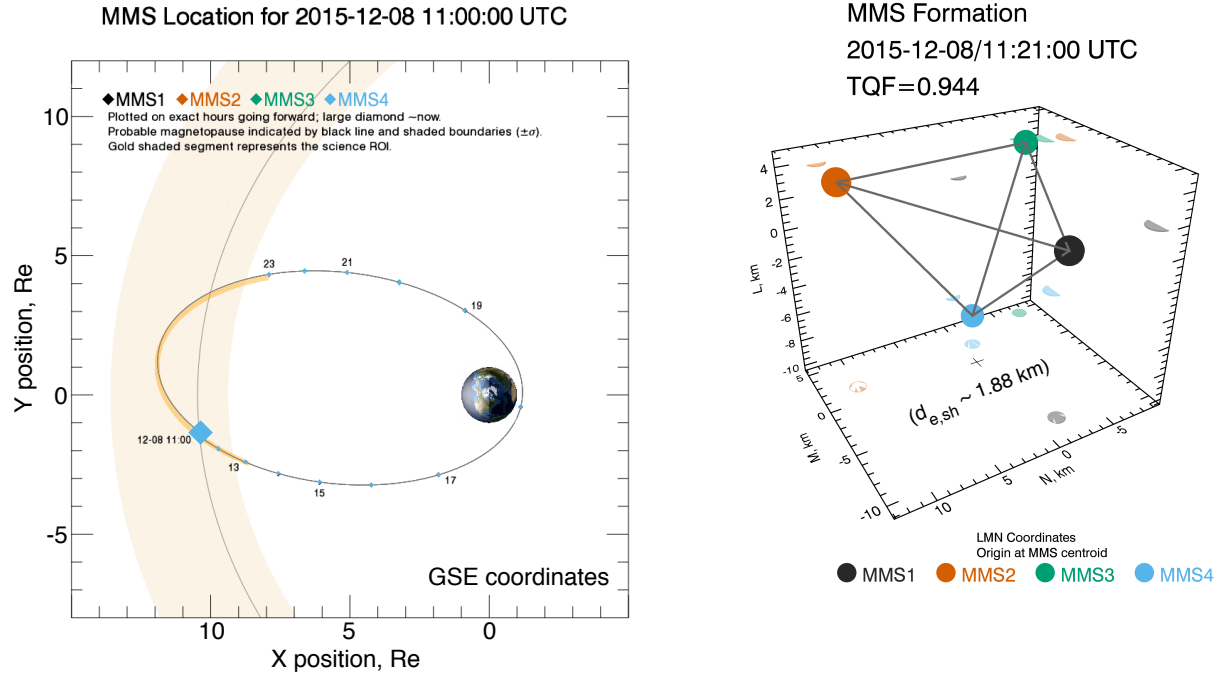


Figure 1: (Left) MMS orbit for 8 December 2015, where the $X_{GSE}-Y_{GSE}$ position of the tetrahedron at 11:00 UT is marked with a blue diamond, and (right) formation of the MMS tetrahedron during the EDR event. The LMN coordinates are defined in the text and taken from *Burch and Phan* [2016].

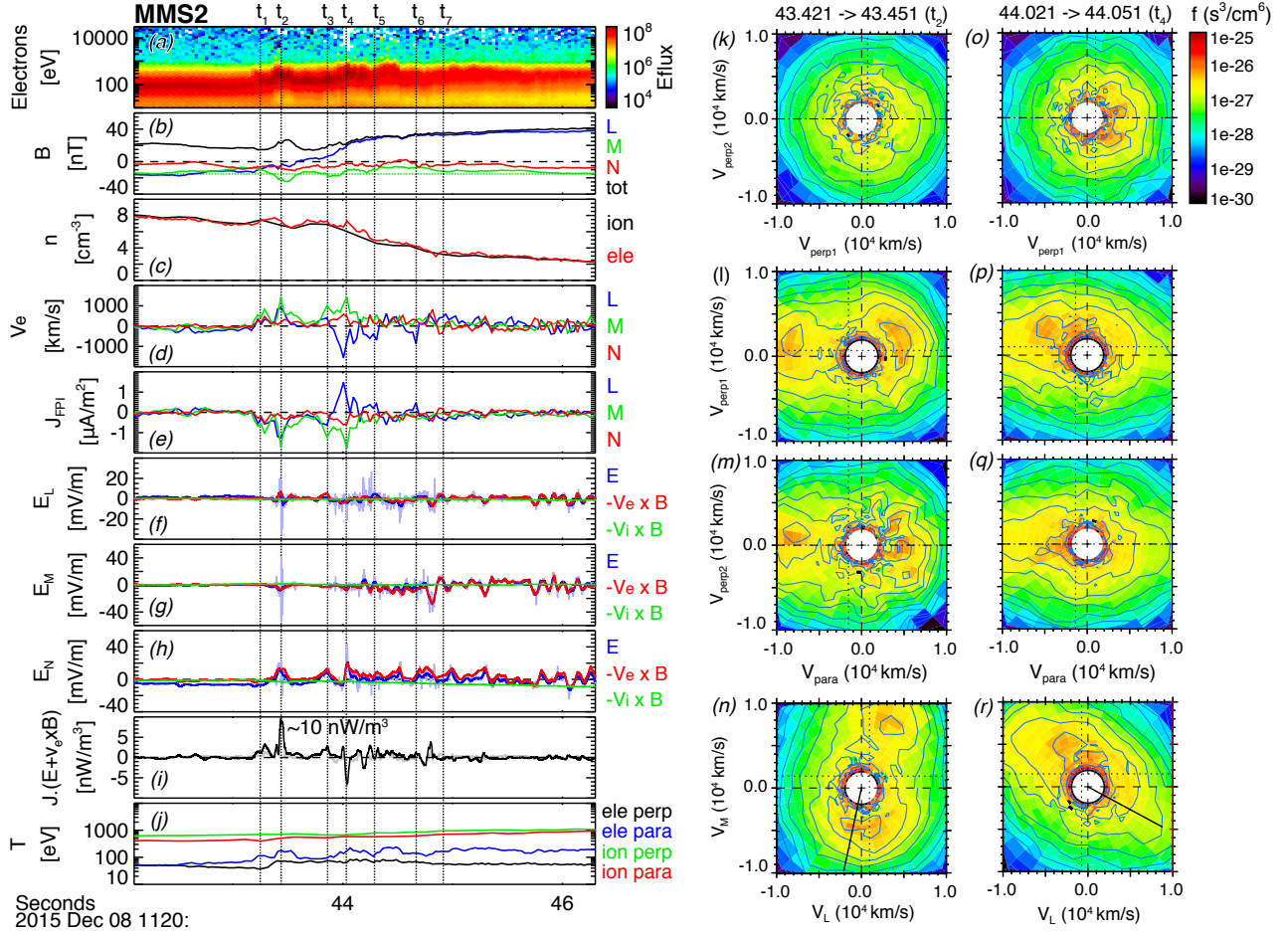


Figure 2: (a) Electron spectrogram, (b) magnetic field vector, (c) plasma densities, (d) electron velocity, (e) current calculated from the plasma data, (f-h) the components of the measured electric field (full-resolution in light blue, smoothed in blue) and the electron (red) and ion (green) convective fields, (i) the work done by the EM field, $\vec{J} \cdot \vec{E}'$, (total in black, $J_L E'_L + J_M E'_M$ in grey), where \vec{J} is calculated from the plasma data, (j) plasma ion and electron temperatures, (k-n) cuts of the eVDF taken at t_2 , (o-r) cuts of the eVDF taken at t_4 . The LMN eigenvectors were taken from *Burch and Phan* [2016] and are listed in Section 2. The solid black lines in (n) and (r) are the local magnetic field vectors projected into the L-M plane.

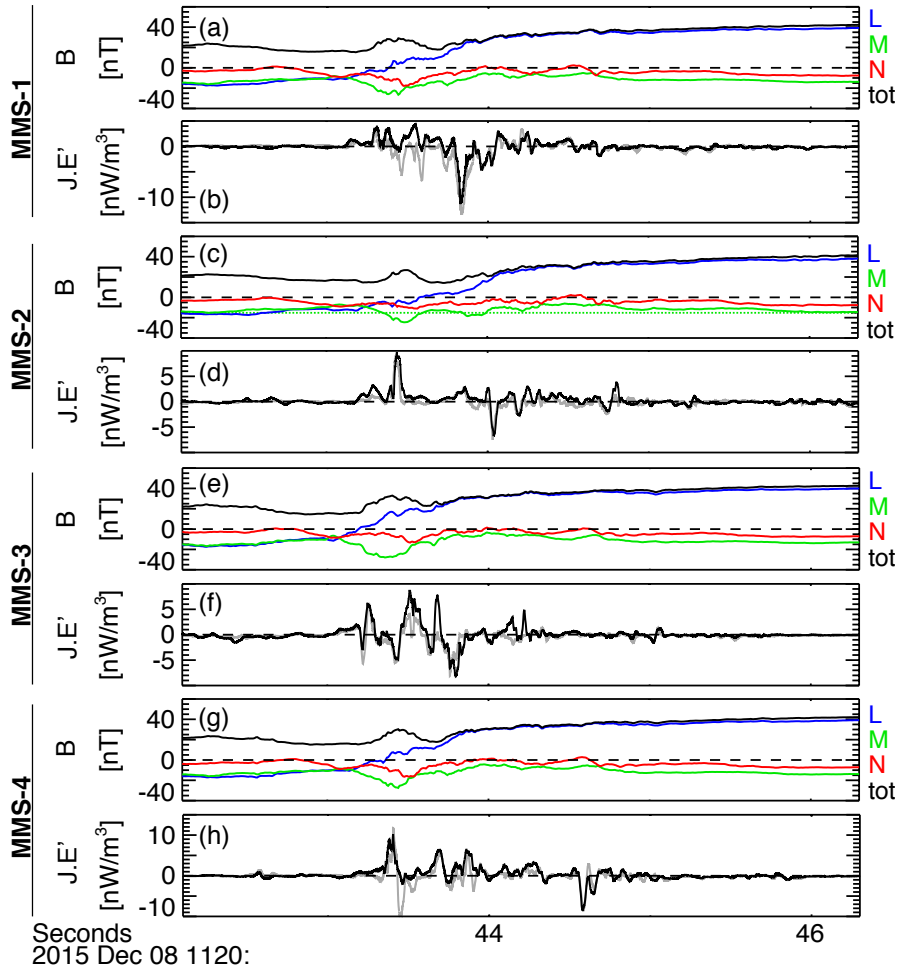


Figure 3: (a, c, e, g) Magnetic field vector and (b, d, f, h) work done by the EM field, $\vec{J} \cdot \vec{E}'$ in black and $J_L E'_L + J_M E'_M$ in grey, for (a-b) MMS1, (c-d) MMS2, (e-f) MMS3, and (g-h) MMS4.

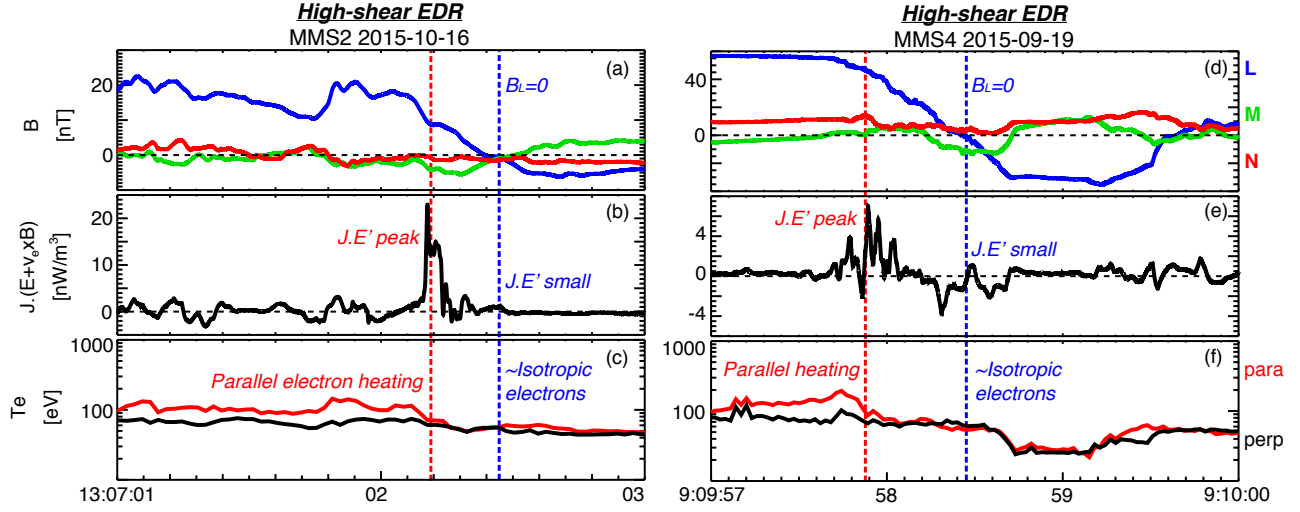


Figure 4: (a, d) Magnetic field vector, (b, e) energy conversion rate in the electron frame, (c, f) parallel (red) and perpendicular (black) electron temperatures for two high-shear EDR events. The left-hand-side panels show the event from 2015-10-16 [Burch *et al.*, 2016]. Right-hand side shows the event from 2015-09-19 [Hwang *et al.*, 2017]. The LMN coordinates systems are taken from the two aforementioned papers. The vertical dashed lines indicate the B_L reversal point (blue) and the electron crescent point (red).

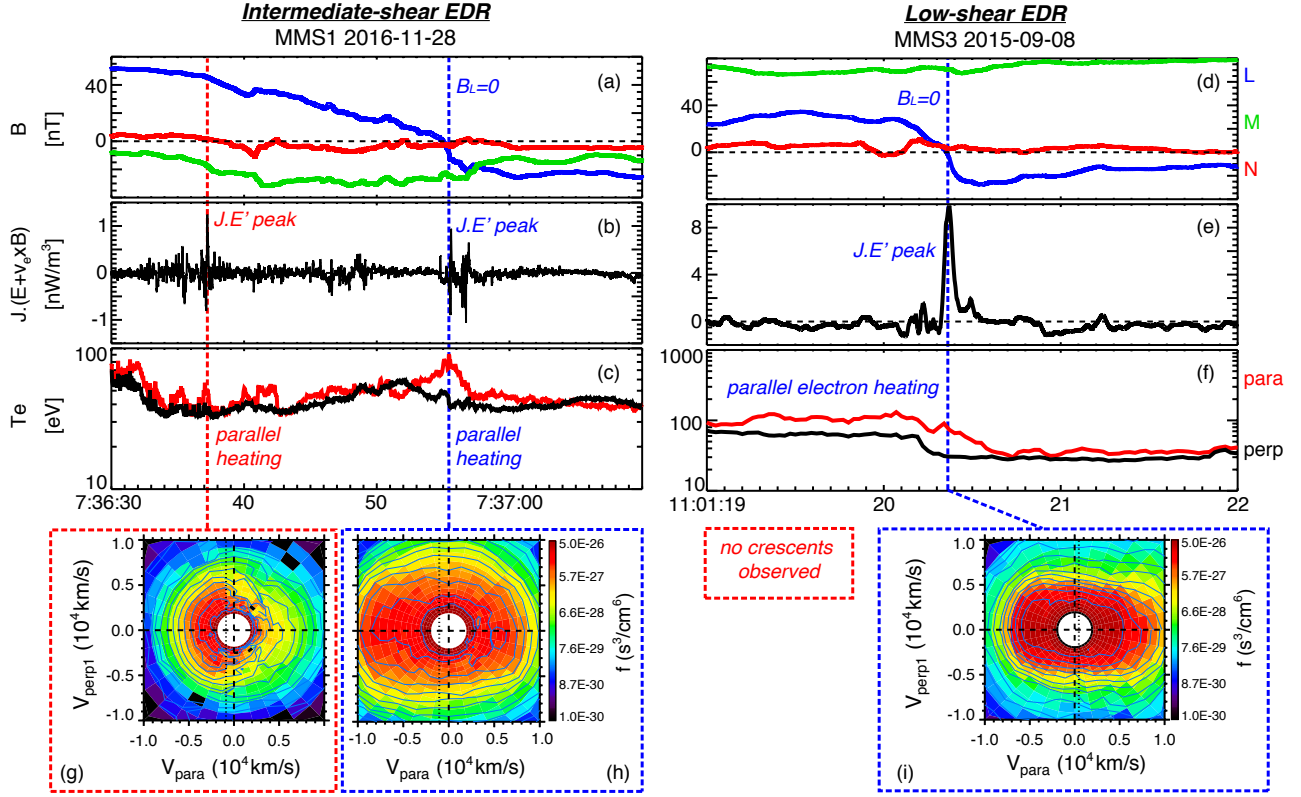


Figure 5: (a, d) Magnetic field vector, (b, e) energy conversion rate in the electron frame, (c, f) parallel (red) and perpendicular (black) electron temperatures for one intermediate-shear EDR event (left) and one low-shear EDR event (right). The left-hand side shows the event from 2016-11-28. The right-hand side shows the event from 2015-09-08 [Eriksson *et al.*, 2016]. The LMN coordinates system for the latter event were taken from Eriksson *et al.* [2016]. The vertical dashed lines indicate the B_L reversal point (blue) and the electron crescent point (red). The LMN coordinate system for the 28 Nov 2016 event was determined by minimization of Faraday residue [Khrabrov and Sonnerup, 1998] of burst electric and magnetic field data from MMS-1 over the interval 18 Nov 2016 7:36:32–7:37:00 UT. In geocentric solar ecliptic (GSE), the LMN system for this event is $L=[0.178, -0.159, 0.971]$, $M=[0.245, -0.9489, -0.200]$, $N=[0.953, 0.273, -0.130]$.